

THE SIGNATURE OF ATMOSPHERIC TIDES IN SUB-DAILY VARIATIONS OF EARTH ROTATION AS UNVEILED BY GLOBALLY-GRIDDED ATMOSPHERIC ANGULAR MOMENTUM FUNCTIONS

M. SCHINDELEGGER¹, J. BÖHM¹, D.A. SALSTEIN², H. SCHUH¹

¹ Institute of Geodesy and Geophysics, Vienna University of Technology
27-29 Gußhausstraße, A-1040 Wien, Austria
e-mail: michael.schindelegger@tuwien.ac.at, johannes.boehm@tuwien.ac.at,
harald.schuh@tuwien.ac.at

² Atmospheric and Environmental Research, Inc.
131, Hartwell Avenue, Lexington, MA 02421-3126, USA
e-mail: salstein@aer.com

ABSTRACT. Thermally-driven atmospheric tides provide a small but distinct contribution to short-period variations of Earth rotation parameters (ERP). The effect of diurnal and semi-diurnal tides, commonly denoted as S_1 and S_2 , respectively, is in the range of 2 - 10 μ s for polar motion and 2 - 10 μ s for changes in length-of-day (LOD). Even though ocean tides represent a much more dominant driving agent for ERP fluctuations at short time scales, high-frequency atmospheric effects are non-negligible, particularly given the prospective measurement accuracy of space geodetic techniques. However, previous studies, such as Brzeziński et al. (2002), de Viron et al. (2005) or Schindelegger et al. (2011), have been noticeably inconclusive on the exact amplitude and phase values of S_1 and S_2 atmospheric excitation signals.

This study aims at shedding light on the origin of these uncertainties with respect to the axial component of Earth's rotation vector by investigating times series of atmospheric angular momentum (AAM) functions that are given on global grids and computed from three-hourly meteorological data of the European Centre for Medium-Range Weather Forecasts (ECMWF). The signature of diurnal and semi-diurnal atmospheric tides is clearly visible in the gridded axial AAM functions, revealing a distinct spatial and temporal phase difference between pressure and wind tidal constituents of about $\pm\pi$. It is shown that due to this counterbalance and the explicit axisymmetric spatial structure of S_1 and S_2 , the net effect in sub-diurnal AAM (which is calculated from the global sum of gridded AAM functions) is always a small quantity, particularly sensitive to minor differences between the analysis fields of numerical weather models.

1. DATA AND METHODOLOGY

The three-hourly meteorological data of this paper originated from the so-called *Atmospheric model delayed cut-off (DCDA)* analysis, which was introduced as a part of a recent re-organization of the ECMWF assimilation system on 29 June 2004. Geopotential, temperature and specific humidity values as well as wind velocities were downloaded as pressure level data at 1° horizontal resolution for the time span 1 January 2010 to 1 July 2010. The preprocessing of the data involved interpolation of all meteorological parameters onto a topography-based reference surface and an appropriate georeferencing of the discrete atmospheric grid.

Based on such a dataset, routine calculation of AAM, which is conventionally split up into pressure and wind terms, requires full spatial integration over pressure p , co-latitude θ and longitude λ . In this study though, we solely performed vertical integration (from the top of the atmospheric model down to the surface pressure p_s) for every 1° by 1° atmospheric column, arriving at the area-weighted grid point-wise contributions to the axial pressure and wind AAM functions χ_3^p and χ_3^w (Schindelegger et al., 2011):

$$\chi_3^p(\theta, \lambda) = \frac{0.757}{C_m} \int_0^{p_s} \frac{r^4}{g} \sin^2 \theta [\sin \theta d\lambda d\theta] dp \quad (1)$$

$$\chi_3^w(\theta, \lambda) = \frac{0.999}{C_m \Omega} \int_0^{p_s} \frac{r^3}{g} u \sin \theta [\sin \theta d\lambda d\theta] dp \quad (2)$$

Herein, C_m is the mantle's polar moment of inertia, Ω denotes the Earth's mean angular velocity and g is the gravity acceleration at geocentric radius r . The decisive quantity for the wind term is the field of zonal wind speed u . Equations (1) and (2) are valid at any single epoch. Hence, considering the entire time span accordingly produced two three-dimensional arrays $\chi_3^p(t, \theta, \lambda)$ and $\chi_3^w(t, \theta, \lambda)$, which were signified as *gridded AAM functions* (pressure and wind terms).

In order to access the contribution of diurnal and semi-diurnal atmospheric tides to the gridded AAM functions, we applied a suitable bandpass filter on the time series of each grid-point at the frequencies of interest, i.e. 1 and 2 cyc/day. As a result, four three-dimensional grids were obtained, featuring the global and regional contributions of the S_1 and S_2 pressure and wind tides to atmospheric excitation of LOD. In a final step, we transformed the half-yearly record of those grids onto a mean day by averaging all fields with common integer hour. The gridded and filtered AAM functions were thus stacked to $\bar{\chi}_3^{p,w}(t, \theta, \lambda)$, with the time vector being reduced to $t = (0, 3, 6, 9, 12, 15, 18, 21)$ UTC. The mean day grids of $\bar{\chi}_3^{p,w}$ provided the backbone of our analysis and are further examined in the next section.

2. ATMOSPHERIC TIDES IN GRIDDED AAM FUNCTIONS

Figure 1 gives an idea of how the S_1 and S_2 pressure and wind tides are represented in the gridded AAM functions at the very first epoch (0 UTC) of the daily mean cycle. A distinct pattern of alternating highs and lows is evident for the semi-diurnal cycle (left part of Figure 1) and one would recognize a westward movement of those signals if further epochs are considered. More importantly, we found a distinct spatial phase difference of $\pm\pi$ between the pressure and zonal wind contributions of S_2 . The right part of Figure 1 reveals a less harmonic and regular structure of the S_1 constituents, and thus no clear spatial phase shift is discernable between the gridded pressure and wind terms. These qualitative findings are in agreement with the predicted behavior of atmospheric tides from simple dynamical models, e.g. the pioneering work of Chapman and Lindzen (1970).

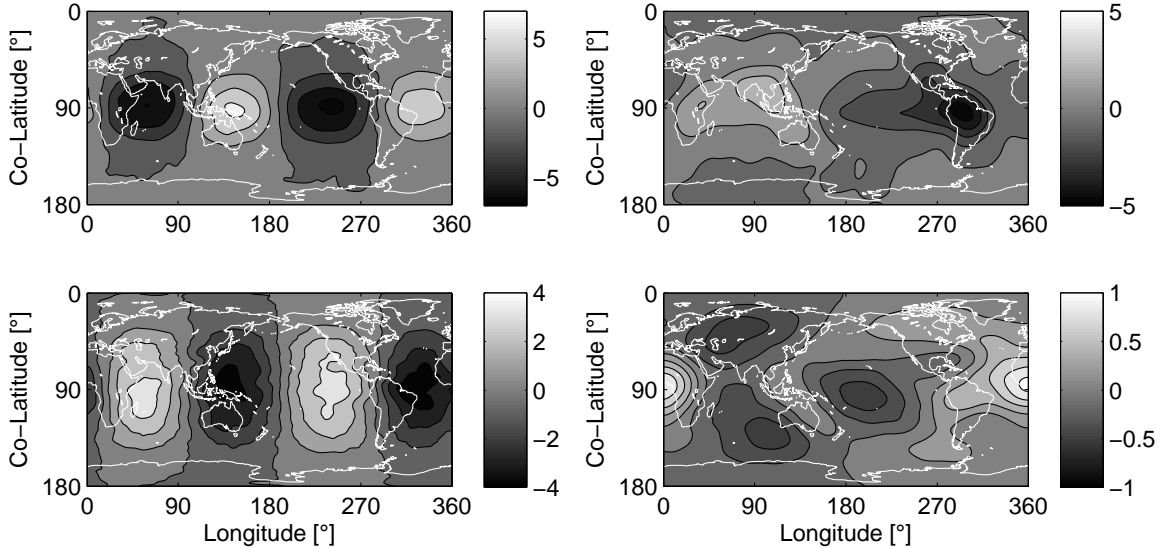


Figure 1: Semi-diurnal and diurnal atmospheric tides as represented by axial gridded AAM functions at 0 UTC. Left part of figure: S_2 pressure term (top half) and S_2 wind term (bottom half). Right part of figure: S_1 pressure term (top half) and S_2 wind term (bottom half). Units are $[\mu s] \cdot 10^{-3}$.

It proved interesting to perform summation over longitude and latitude for each field of $\bar{\chi}_3^{p,w}(t, \theta, \lambda)$, thus looking at the epoch-wise net effect of the gridded and filtered AAM functions. The resulting mean

day variations of S_1 and S_2 are displayed in Figure 2, split up into a pressure portion, a wind portion and the total effect on excitation of LOD. For both tidal bands, the wind term shows a phase lag of about 6 hours with respect to the pressure term. This phenomenon prompts the semi-diurnal wind term to largely balance the respective contribution of the pressure term, so that the total net effect at S_2 remains a smaller quantity throughout.

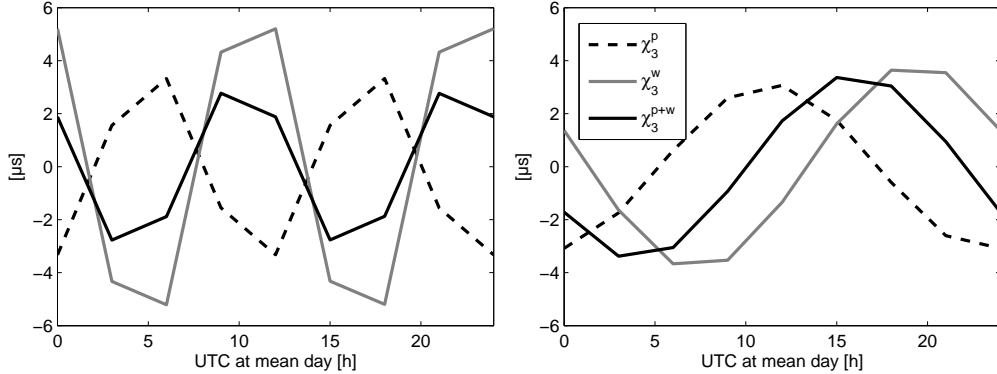


Figure 2: Daily mean variations of the S_2 (left figure) and S_1 (right figure) signals in atmospheric excitation of LOD, calculated from three-hourly gridded AAM functions. Pressure term (*dashed black line*) and wind term (*gray line*) add up to the total excitation signal (*solid black line*).

We tried to address the nature of signals depicted in Figure 2 by focusing on the gridded AAM functions in the semi-diurnal band. In detail, the origin of the epoch-wise net effect and the prevailing counterbalance of pressure and wind effects as illustrated in Figure 2 were investigated. At first, we discerned that the first-order approximation of the global grids of $\overline{\chi}_3^{p,w}(t, \theta, \lambda)$ is an axisymmetric structure corresponding to a spherical harmonic of degree and order $n = m = 2$. However, precisely due to its axisymmetry, this $n = m = 2$ component possesses a vanishing net effect, and it was therefore removed from the gridded pressure and wind terms at each epoch by means of a least squares fit and subsequent subtraction. The resulting pressure term at 0 UTC (Figure 3) reveals regionally distributed residuals, most notably over the Pacific and the Indian Ocean. Both anomalies are negative and therefore amplify the associated semi-diurnal pressure lows in Figure 1, so that the net effect at 0 UTC is negative, cf. the pressure term values in the left part of Figure 2. This assertion is supported by a dominating negative bulge in the cumulated meridional profile, which was obtained from $\overline{\chi}_3^p(t, \theta, \lambda)$ after summation over longitude.

An equivalent analysis was carried out for the gridded wind term at 0 UTC, see Figure 4. Removal of the symmetric $n = m = 2$ component again revealed notable residuals in the Pacific band from $\lambda = 150^\circ$ to about 300° , which account for a positive value in the global net effect, cf. the wind term values in the left part of Figure 2. The associated meridional profile of $\overline{\chi}_3^w(t, \theta, \lambda)$ shows two main positive bulges located at temperate latitudes.

3. DISCUSSION AND CONCLUSION

By investigating gridded AAM functions at three-hourly resolution for the time period 1 January 2010 to 1 July 2010, we found that the primary diurnal and semi-diurnal pressure and wind signals of atmospheric tides, which are associated with harmonic coefficients of degree and order 1 and degree and order 2, respectively, do not contribute to excitation of LOD. Instead, small secondary pressure and wind effects are decisive for changes in the axial component of AAM. It is highly likely that those residuals are represented differently in the analysis fields of each atmospheric model. In particular for the semi-diurnal cycle, the relevant anomalies can be interpreted as amplifications of the pressure and wind highs and lows over the same latitude band, located in the Pacific region. Considering this and the fact that the barometric S_2 tide features a distinct spatial phase difference of $\pm\pi$ with respect to the S_2 wind tide, it is understandable that the resulting excitation time series of pressure and wind terms are almost exactly out-of-phase and thus largely counterbalance each other.

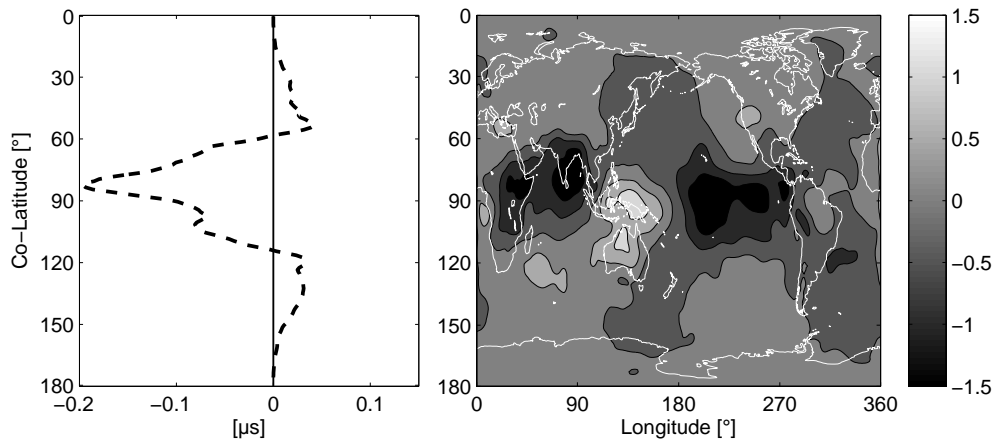


Figure 3: Right figure: gridded pressure term at 0 UTC after removal of the symmetric tidal signal of degree and order 2. Units are $[\mu\text{s}]\cdot 10^{-3}$. Left figure: corresponding longitudinal sum of the pressure term at 0 UTC.

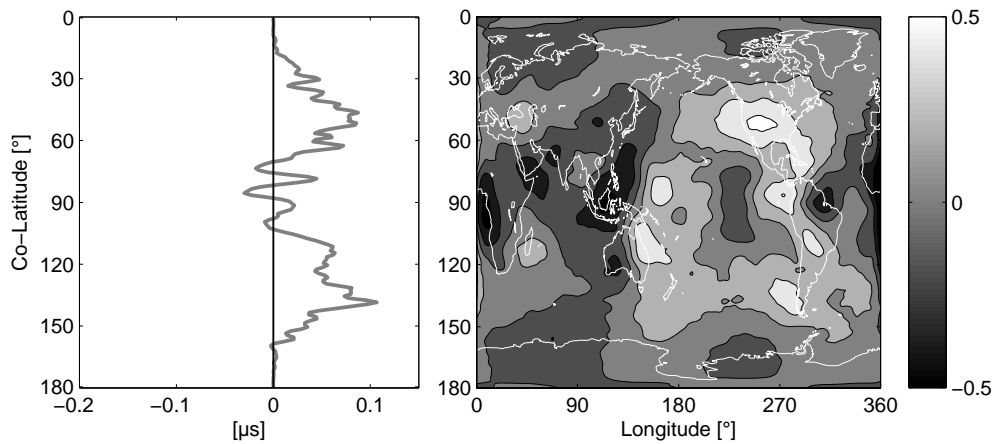


Figure 4: Right figure: gridded wind term at 0 UTC after removal of the symmetric tidal signal of degree and order 2. Units are $[\mu\text{s}]\cdot 10^{-3}$. Left figure: corresponding longitudinal sum of the wind term at 0 UTC.

Acknowledgements. This study was carried out within project P20902-N10 of the Austrian Science Fund. David Salstein was also supported by the US National Science Foundation under Grant ATM-0913780.

4. REFERENCES

- Brzeziński, A., Bizouard, C., Petrov, S.D. Influence of the atmosphere on Earth rotation: What new can be learned from the recent atmospheric angular momentum estimates? *Surveys in Geophysics*, 23:33-69, 2002.
- Chapman, S. and Lindzen, R.S. *Atmospheric Tides: Thermal and Gravitational*. Reidel, Dordrecht, The Netherlands, 1970.
- de Viron, O., Schwarzbaum, G., Lott, F., Dehant, V. Diurnal and semi-diurnal effects of the atmosphere on the Earth rotation and geocenter motion. *J. Geophys. Res.*, 110(B11404), 2005.
- Schindelegger M., Böhm J., Salstein D., Schuh H. High-resolution atmospheric angular momentum functions related to Earth rotation parameters during CONT08. *J. Geod.*, 85(7), pp. 425-433, 2011.